

# Proposal of a new quantum annealing schedule for studying transverse-field-based quantum versus classical annealing of the Ising model: a case study of the Ising spin glass model on the square lattice by the Monte Carlo simulation

Chiaki Yamaguchi\*

Tokyo Quantum Computing, Haramura 17217-1689, Suwagun,  
Nagano 391-0115, Japan

## Abstract

Recently, Heim, Rønnow, Isakov and Troyer [*Science* **348** (2015) 215] have reported that Monte Carlo simulations for the Ising spin glass model on the square lattice in the physically relevant continuous-imaginary-time limit do not show superiority of quantum annealing (QA) using transverse field against classical annealing (CA). Although the QA schedule that they had used has been using conventionally, however the QA schedule mathematically has no guarantee that the used schedule is the best QA schedule for performance of optimization. We propose a new QA schedule for studying transverse-field-based quantum versus classical annealing of the Ising model. The present QA schedule is made based on the concept of perturbation theory. This QA schedule utilizes a smallest effective transverse field derived in this article. As a case study, we study QA of the Ising spin glass model on the square lattice at low but finite temperature. A new Monte Carlo algorithm using the physically relevant continuous-imaginary-time limit is performed. As the simulation results, we show superiority of QA against CA when the annealing time is spent enough.

## 1 Introduction

The quantum annealing (QA) is an optimization method utilizing quantum effect[1, 2, 3, 4, 5]. By using QA, the solutions of given optimized problems are approximately or exactly obtained. QA is also related to a quantum computation by adiabatic evolution[6, 7].

---

\*Email:info@to-qc.com

QA is proposed as an alternative of the classical annealing (CA)[8]. In CA, the temperature is operated from high to low in order to utilize thermal fluctuations. On the other hand, in QA, an external field generating quantum effect is operated from large to zero in order to utilize quantum fluctuations. These annealings help to make the systems escape from local minima of the free energy, and the systems reach low-energy states effectively.

The understandings of QA are recently becoming significant in relation to the D-Wave chip[9]. This chip is designed to perform QA for solving optimization problems. The occurrence of quantum properties for this chip is shown[9].

We simulate QA of real-physical systems in this article, and we do not simulate QA as a classical optimization method in this article. Recently, it is reported in Ref. [10] that Monte Carlo simulations for the Ising spin glass model on the square lattice in the physically relevant continuous-imaginary-time limit do not show superiority of QA using transverse field against CA. In order to study physically relevant systems, we use a continuous-imaginary-time quantum Monte Carlo algorithm in this article. In addition, we investigate the Ising spin glass model on the square lattice.

Although the QA schedule used in Ref. [10] has been using conventionally, however the QA schedule mathematically has no guarantee that the used schedule is the best QA schedule for performance of optimization. We propose a new QA schedule for studying transverse-field-based quantum versus classical annealing of the Ising model. This QA schedule utilizes a smallest effective transverse field derived in this article. We derive this field based on a discussion of percolation of spin correlation for the continuous-imaginary-time direction of one spin. The present QA schedule is made based on the concept of perturbation theory. Here, the concept of perturbation theory means the comparison between the system with no transverse field and the system with the smallest effective transverse field. By this comparison, the superiority of QA (or CA) can be made clear.

We also propose a quantum Monte Carlo algorithm using the physically relevant continuous-imaginary-time limit. This algorithm is a Glauber-dynamics-like algorithm (a heat-bath-like algorithm) which performs single-spin flips in the real space and cluster flips in the imaginary-time space. When the transverse field is not imposed, this algorithm becomes the Glauber dynamics. The Glauber dynamics is suited to the study of the dynamical features of physical systems[11, 12]. The present algorithm is a new one. The orders of calculation costs for the present algorithm and the related algorithms [13, 14] can be the same for the system size. The differences between the present algorithm and the related algorithms are mentioned in this article. The mathematical form of the present Monte Carlo algorithm is directly related to the derivation of a smallest effective transverse field derived in this article, thus we use the present Monte Carlo algorithm in this article.

We compare three annealings: the present one, a conventional quantum one and a classical one. The simulation results for the annealings are shown in this article.

This article is organized as follows. The quantum annealing and the spin

glass model are explained in §2. The present algorithm is derived in §3. If readers do not have interest in the derivation of the algorithm, the readers can skip §3. The way of the application of the present algorithm is written in §4. The differences between the present algorithm and the related algorithms are mentioned in §4. Quantities that we treat in this article are described in §5. A smallest effective transverse field is derived in §6. A new QA schedule is proposed in §6. Simulation results are shown in §7. Concluding remarks are in §8.

## 2 The quantum annealing and the spin glass model

The quantum annealing can be to investigate a time dependent Hamiltonian  $\mathcal{H}(t)$  which has quantum effect terms. Usually, the Hamiltonian  $\mathcal{H}(t)$  can be written as

$$\mathcal{H}(t) = J(t)\mathcal{H}_P + \gamma(t)\mathcal{H}_Q, \quad (1)$$

where  $t$  is the time from  $t = 0$  to  $t = T_I$ .  $\mathcal{H}_P$  is the problem Hamiltonian that an optimization problem is written.  $\mathcal{H}_Q$  is a quantum effect Hamiltonian.  $J(t)$  is a increasing function for  $t$ , or  $J(t)$  is a constant.  $J(t)$  increases from 0 to 1 for example.  $\gamma(t)$  is a decreasing function for  $t$ .  $\gamma(t)$  decreases from a large value to 0 for example, or  $\gamma(t)$  decreases from 1 to 0 for example. A method using a pulse of the transverse field is also proposed[14].

The problem Hamiltonian  $\mathcal{H}_P$  is written as the form of the Ising spin glass model called the Edwards-Anderson model. The Hamiltonian  $\mathcal{H}_P$  is given by [15, 16, 17, 18]

$$\mathcal{H}_P = - \sum_{\langle ij \rangle} \tau_{ij} S_i S_j, \quad (2)$$

where  $\langle ij \rangle$  denotes nearest-neighbor pairs,  $S_i$  is a state of the spin at site  $i$ , and  $S_i = \pm 1$ . The value of  $\tau_{ij}$  is given by the problem that is asked to solve. In the spin glass model, the probability giving the value of  $\tau_{ij}$  is

$$P(\tau_{ij}) = \frac{1}{2}\delta_{\tau_{ij},-1} + \frac{1}{2}\delta_{\tau_{ij},1} \quad (3)$$

for example. We use the value of  $\tau_{ij}$  obtained by using Eq. (3) in this article. The model using  $P(\tau_{ij})$  is especially called the  $\pm J$  Ising spin glass model.

The quantum effect Hamiltonian  $\mathcal{H}_Q$ , which is investigated in this article, is given by [1, 3, 4, 5]

$$\mathcal{H}_Q = - \sum_{i=1}^N \sigma_i^x, \quad (4)$$

where  $\sigma_i^k$  is the  $k$  component of the Pauli matrix at site  $i$ .  $N$  is the number of sites in the whole system. The Pauli matrices are

$$\sigma^x = \begin{pmatrix} 0 & 1 \\ 1 & 0 \end{pmatrix}, \quad \sigma^y = \begin{pmatrix} 0 & -i \\ i & 0 \end{pmatrix} \quad \text{and} \quad \sigma^z = \begin{pmatrix} 1 & 0 \\ 0 & -1 \end{pmatrix}. \quad (5)$$

By using Eqs.(1), (2) and (4), the Hamiltonian  $\mathcal{H}(t)$  is also written as

$$\mathcal{H}(t) = -J(t) \sum_{\langle ij \rangle} \tau_{ij} \sigma_i^z \sigma_j^z - \gamma(t) \sum_{i=1}^N \sigma_i^x. \quad (6)$$

We study this Hamiltonian  $\mathcal{H}(t)$ .

### 3 The derivation of a new continuous-imaginary-time quantum Monte Carlo algorithm

We derive the present algorithm. The way of applying the algorithm is described in §4.

The Glauber dynamics is suited to the study of the dynamical features of physical systems[11, 12]. By applying the Glauber dynamics, discussions for dynamical features as a physical system are possible[11, 12]. The Glauber dynamics is a heat-bath algorithm for the Ising model. We propose a Glauber-dynamics-like algorithm (a heat-bath-like algorithm) which performs single-spin flips in the real space and cluster flips in the imaginary-time space. For the real-space direction, the present algorithm performs single-spin flips like as the Glauber dynamics does. The present algorithm performs cluster flips for the imaginary-time direction. For the imaginary-time direction, the continuous-imaginary-time limit is applied.

We use the Suzuki-Trotter decomposition given by [19]

$$e^{-\beta(\mathcal{H}_A + \mathcal{H}_B + \mathcal{H}_C)} = \lim_{\Delta\tilde{t} \rightarrow 0} (e^{-\mathcal{H}_A \Delta\tilde{t}} e^{-\mathcal{H}_B \Delta\tilde{t}} e^{-\mathcal{H}_C \Delta\tilde{t}})^{\frac{\beta}{\Delta\tilde{t}}}, \quad (7)$$

where  $\Delta\tilde{t} \equiv \frac{\beta}{M}$ ,  $M$  is called the Trotter number, and  $\tilde{t}$  is called the imaginary time.  $\beta$  is the inverse temperature,  $\beta = 1/k_B T_E$ ,  $T_E$  is the temperature, and  $k_B$  is the Boltzmann constant. The physically relevant continuous-imaginary-time limit mentioned in Ref. [10] corresponds to the limit of  $\Delta\tilde{t} \rightarrow 0$  in this article. By this decomposition, the  $d$ -dimensional quantum system is treated as the  $d+1$ -dimensional classical system. Since a continuous-imaginary-time quantum Monte Carlo algorithm is used in this study, the system for  $\Delta\tilde{t} \rightarrow 0$  is directly investigated, and this study is not affected by the error of this decomposition. There is a relation[19]:

$$\langle \sigma_x^z | e^{\beta\gamma(t)\sigma^x} | \sigma_y^z \rangle = \frac{1}{2} (e^{\beta\gamma(t)} + \sigma_x^z \sigma_y^z e^{-\beta\gamma(t)}), \quad (8)$$

where  $\sigma_x^z, \sigma_y^z = \pm 1$ . Thus, the partition function  $Z(t)$  is written as [19]

$$\begin{aligned} Z(t) = & \lim_{\Delta\tilde{t} \rightarrow 0} \sum_{\{\sigma_{ik}^z\}} \exp \left\{ J(t) \Delta\tilde{t} \sum_{k \in \rho} \sum_{ij \in \rho} \tau_{ij} \sigma_{ik}^z \sigma_{jk}^z \right. \\ & \left. + \sum_{kl \in \rho} \sum_{i \in \rho} \log \frac{\exp(\gamma(t) \Delta\tilde{t}) + \sigma_{ik}^z \sigma_{il}^z \exp(-\gamma(t) \Delta\tilde{t})}{2} \right\}, \quad (9) \end{aligned}$$

where  $\rho$  is the set of the coordinates of the weights for the decomposed partition function in the  $d + 1$  classical system. The coordinates of  $\rho$  is somewhat complicated[19], but there is no need to understand the coordinates, because of taking the continuous-imaginary-time limit. By performing  $\Delta\tilde{t} \rightarrow 0$ , the imaginary time becomes a continuous space. In Eq. (9), the term for  $\sigma_{ik}^z \sigma_{jk}^z$  is a term for the interaction of real-space direction, and the term for  $\sigma_{ik}^z \sigma_{il}^z$  is a term for the interaction of imaginary-time direction. The imaginary-time direction has periodic boundary conditions. The size of the imaginary-time direction is the same with the inverse temperature  $\beta$ . Eq. (9) is also written for  $\Delta\tilde{t} \rightarrow 0$  as

$$Z(t) = \lim_{\Delta\tilde{t} \rightarrow 0} \sum_{\{\sigma_{ik}^z\}} \exp \left[ J(t) \Delta\tilde{t} \sum_{k \in \rho} \sum_{ij \in \rho} \tau_{ij} \sigma_{ik}^z \sigma_{jk}^z + \log(\gamma(t) \Delta\tilde{t}) \sum_{kl \in \rho} \sum_{i \in \rho} \frac{1 - \sigma_{ik}^z \sigma_{il}^z}{2} \right]. \quad (10)$$

In order to derive the present algorithm, we derive weights for graph representation. The framework of deriving weights for graph representation is described in Ref. [20]. We define the weight of two spins for imaginary-time direction as  $w(\sigma_{ik}^z, \sigma_{il}^z)$ .  $w(\sigma_{ik}^z, \sigma_{il}^z)$  is given by

$$w(\sigma_{ik}^z, \sigma_{il}^z) = \exp \left[ \log(\gamma(t) \Delta\tilde{t}) \frac{1 - \sigma_{ik}^z \sigma_{il}^z}{2} \right]. \quad (11)$$

We define the weight for  $\sigma_{ik}^z \sigma_{il}^z = 1$  as  $w_{\text{para}}$ . We obtain

$$w_{\text{para}}(\sigma_{ik}^z, \sigma_{il}^z) = 1. \quad (12)$$

We define the weight for  $\sigma_{ik}^z \sigma_{il}^z = -1$  as  $w_{\text{anti}}$ . We obtain

$$w_{\text{anti}}(\sigma_{ik}^z, \sigma_{il}^z) = \gamma(t) \Delta\tilde{t}. \quad (13)$$

We define the weight of graph for connecting two spins as  $w(g_{\text{conn}})$ . We define the weight of graph for cutting two spins as  $w(g_{\text{cut}})$ . We are able to write

$$w_{\text{para}}(S_i, S_j, J_{i,j}) = w(g_{\text{conn}}) + w(g_{\text{cut}}), \quad (14)$$

and

$$w_{\text{anti}}(S_i, S_j, J_{i,j}) = w(g_{\text{cut}}). \quad (15)$$

By using Eqs. (12), (13), (14) and (15), we obtain

$$w(g_{\text{conn}}) = 1 - \gamma(t) \Delta\tilde{t}, \quad (16)$$

and

$$w(g_{\text{cut}}) = \gamma(t) \Delta\tilde{t}. \quad (17)$$

We define the probability of cutting two spins for  $\sigma_{ik}^z \sigma_{il}^z = 1$  as  $P_{\text{para}}(g_{\text{cut}})$ . We define the probability of cutting two spins for  $\sigma_{ik}^z \sigma_{il}^z = -1$  as  $P_{\text{anti}}(g_{\text{cut}})$ . We are able to write

$$P_{\text{para}}(g_{\text{cut}}) = \frac{w(g_{\text{cut}})}{w(g_{\text{conn}}) + w(g_{\text{cut}})} = \gamma(t) \Delta\tilde{t}, \quad (18)$$

and

$$P_{\text{anti}}(g_{\text{cut}}) = \frac{w(g_{\text{cut}})}{w(g_{\text{cut}})} = 1. \quad (19)$$

We calculate the number of cuts for  $P_{\text{para}}(g_{\text{cut}})$  of Eq. (18) in the continuous-imaginary-time limit. We define  $n_{\text{add}}$  as the number of cuts for parallel spins  $\sigma \sigma' = 1$  on the continuous-imaginary time per spin. By using Eq. (18), the probability  $P(n_{\text{add}})$  that gives  $n_{\text{add}}$  is obtained as

$$\begin{aligned} P(n_{\text{add}}) &= \lim_{\Delta \tilde{t} \rightarrow 0} \binom{\frac{\beta}{\Delta \tilde{t}} - n_{\text{kink}}}{n_{\text{add}}} (1 - P_{\text{para}})^{\frac{\beta}{\Delta \tilde{t}} - n_{\text{kink}} - n_{\text{add}}} (P_{\text{para}})^{n_{\text{add}}} \\ &= \frac{1}{n_{\text{add}}!} (\gamma(t)\beta)^{n_{\text{add}}} \exp(-\gamma(t)\beta), \end{aligned} \quad (20)$$

where  $\binom{x}{y} \equiv \frac{x!}{y!(x-y)!}$ , and  $n_{\text{kink}}$  is the number of kinks on the imaginary-time per spin. The kink means the position of  $\sigma \sigma' = -1$  on the imaginary time. The position  $\tilde{t}_{\text{add}}$  of the cut for parallel spins  $\sigma \sigma' = 1$  on the continuous-imaginary time is obtained by

$$\tilde{t}_{\text{add}} = \beta R, \quad (21)$$

where  $R$  is a pseudorandom number for  $0 \leq R < 1$ . By using Eq. (19), cuts are added for antiparallel spins  $\sigma \sigma' = -1$  on the imaginary time with probability one. Thus the number of cuts for antiparallel spins on the imaginary time per spin is  $n_{\text{kink}}$ . Therefore, the number of all cuts on the continuous-imaginary time per spin,  $n_{\text{cut}}$ , is given by

$$n_{\text{cut}} = n_{\text{add}} + n_{\text{kink}}. \quad (22)$$

The present algorithm performs single-spin flips in the real space. The transition probability  $P(E \rightarrow E')$  for the energy transition  $E \rightarrow E'$  is given by

$$P(E \rightarrow E') = \frac{e^{-\beta E'}}{e^{-\beta E} + e^{-\beta E'}}. \quad (23)$$

Since cuts are added for the imaginary-time direction, the spin correlations on the imaginary time are cut at the positions of the cuts. Therefore,  $P(E \rightarrow E')$  is only calculated for real spaces. When there is no cut, the present algorithm becomes the Glauber dynamics.

## 4 The way of the application of the present Monte Carlo algorithm

We describe the way of the application of the present algorithm that we propose in this article. The derivation of the present algorithm is in §3. When the transverse field is not imposed, this algorithm becomes the Glauber dynamics.

One Monte Carlo step (sweep) is as follows:

1. The number of cuts for parallel spins on the imaginary time,  $n_{\text{add}}$ , is calculated by using Eq. (20) for each spin, and the positions of cuts for parallel spins on the imaginary time,  $\tilde{t}_{\text{add}}$ , are calculated  $n_{\text{add}}$  times by using Eq. (21) for each spin. Moreover, cuts are placed on all kinks with probability one (Eq. (19)). Clusters are detected by all the cuts. The number of clusters,  $N_C$ , is counted up.
2. The detected clusters are randomly picked up, and the clusters are flipped with the probability of Eq. (23). The trials of flipping clusters are performed  $N_C$  times.
3. The placed cuts are deleted.
4. Quantities are sampled if needing to sample the quantities.

One Monte Carlo step is a unit of time. This time is called the Monte Carlo time. We simulate physical systems for evolution of this time.

Fig. 1 shows a sketch of one Monte Carlo step. Full lines correspond to world-line segments with spin up, and broken lines correspond to worldline segments with spin down. The horizontal axis indicates the real space, and the longitudinal axis indicates the imaginary time. A discrete space is assumed for the real-space direction, and a continuous space is assumed for the imaginary-time direction. The imaginary-time direction has the periodic boundary conditions. (a) Spin states are shown. (b) Cuts are added. Cuts for kinks are represented as bars, and cuts for parallel spins on the imaginary time are represented as crosses. Cuts for kinks are added with the probability one according to Eq. (19). Cuts for parallel spins on the imaginary time are added according to Eqs.(20) and (21). (c) Cluster flips are performed. One of clusters is randomly picked up, and the cluster is flipped with the probability of Eq. (23). Cluster flips are tried for the number of clusters. (d) Cuts are deleted, and quantities are sampled.

Fig. 2 shows a sketch of one cluster flip. The horizontal axis indicates the real space, and the longitudinal axis indicates the imaginary time. (a) Spin states are shown before a cluster  $C_1$  is flipped. (b) Spin states are shown after the cluster  $C_1$  was flipped. If the transition probability  $P(E \rightarrow E')$  of Fig. 2 is calculated,  $P(E \rightarrow E')$  is obtained as  $P(E \rightarrow E') = 1/\{1 + \exp[-2J(t)(\tilde{t}_1 - \tilde{t}_3)\tau_{12} + 2J(t)(\tilde{t}_1 - 2\tilde{t}_2 + \tilde{t}_3)\tau_{23}]\}$ .

One simulation is as follows:

1. A problem (a set of  $\tau_{ij}$ ) is prepared.
2. Initial states of spins at  $t = 0$  are made by using some Monte Carlo steps, and  $t \leftarrow t + 1$  is executed.
3. One Monte Carlo step is performed. Then quantities are sampled for  $t$ , and  $t \leftarrow t + 1$  is executed.
4. When  $t = T_I + 1$ , the simulation is closed.

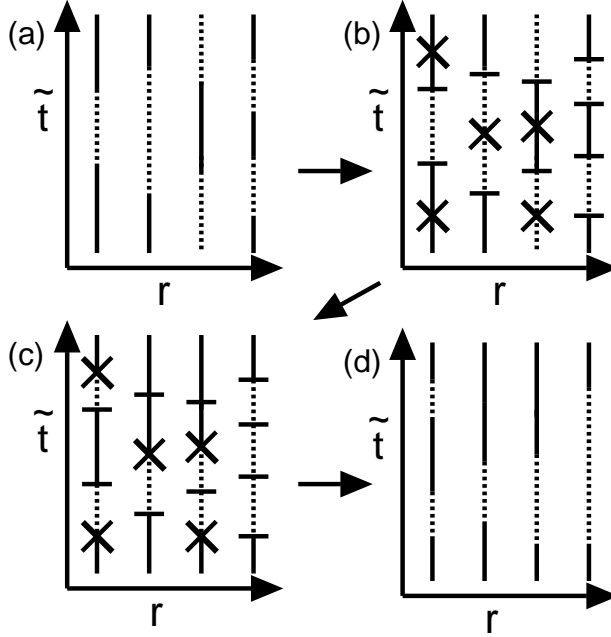


Figure 1: A sketch of one Monte Carlo step. Full lines correspond to worldline segments with spin up, and broken lines correspond to worldline segments with spin down. The horizontal axis indicates the real space, and the longitudinal axis indicates the imaginary time. (a) Spin states are shown. (b) Cuts are added. Cuts for kinks are represented as bars, and cuts for parallel spins on the imaginary time are represented as crosses. (c) Cluster flips are performed. (d) Cuts are deleted, and quantities are sampled.

By repeating the above procedures, many simulations are performed, and the average values of quantities are calculated.

We describe the differences between related algorithms. The algorithm by Rieger and Kawashima is that for each site one generates new cuts in addition to the old ones from the already existing segments via a Poisson process with decay time  $1/\gamma$  along the imaginary time direction[13]. The algorithm proposed directly detects the correlation length along the imaginary time direction. On the other hand, the present algorithm directly treats the number of cuts for detecting the correlation lengths along the imaginary time direction. The present algorithm generates the number of cuts for each site, and the present algorithm adds the cuts onto the imaginary time randomly. The algorithm by Morita, Suzuki and Nakamura is that the initial cluster state is made by giving the position of cuts by the Poisson process with the mean value  $\beta\gamma$  [14]. If the number of generated cuts is odd, one of the cuts is removed to obey the periodic

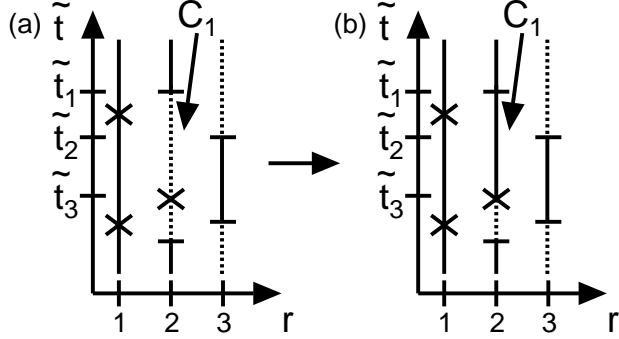


Figure 2: A sketch of one cluster flip. The horizontal axis indicates the real space, and the longitudinal axis indicates the imaginary time. (a) Spin states are shown before a cluster  $C_1$  is flipped. (b) Spin states are shown after the cluster  $C_1$  was flipped.

boundary conditions along the imaginary-time direction[14]. The present algorithm does not judge whether the number of generated cuts is odd or even. The simulation results by these algorithms can be the same for all situations. The orders of calculation costs for the present algorithm and the related algorithms can also be the same, thus we do not compare the algorithms in detail in this article. The aim of the present article is to propose a new quantum annealing schedule and to investigate the efficiency of the schedule. The mathematical form of the present Monte Carlo algorithm is directly related to the derivation of a smallest effective transverse field, and the schedule that we propose in this article utilizes the field. We derive the field in §6.

## 5 Quantities

We describe quantities that we investigate in this article.

By using Eq. (10), the expectation value  $[\langle E \rangle_T]_J$  of the energy  $E$  of the Hamiltonian  $\mathcal{H}(t)$  (Eq. (6)) is written as

$$\begin{aligned}
 [\langle E \rangle_T]_J &= -\frac{\partial}{\partial \beta} [\log Z]_J \\
 &= \left[ \frac{1}{Z} \lim_{\Delta \hat{t} \rightarrow 0} \sum_{\{\sigma_{ik}^z\}} \left( -\frac{J(t)}{M} \sum_{k \in \rho} \sum_{ij \in \rho} \tau_{ij} \sigma_{ik}^z \sigma_{jk}^z - \frac{1}{\beta} \sum_{kl \in \rho} \sum_{i \in \rho} \frac{1 - \sigma_{ik}^z \sigma_{il}^z}{2} \right) \right. \\
 &\quad \left. \times \exp \left[ J(t) \Delta \hat{t} \sum_{k \in \rho} \sum_{ij \in \rho} \tau_{ij} \sigma_{ik}^z \sigma_{jk}^z + \log(\gamma(t) \Delta \hat{t}) \sum_{kl \in \rho} \sum_{i \in \rho} \frac{1 - \sigma_{ik}^z \sigma_{il}^z}{2} \right] \right]_J, \tag{24}
 \end{aligned}$$

where  $\langle \rangle_T$  is the thermal average, and  $[\ ]_J$  is the average for  $\tau_{ij}$ .  $[\ ]_J$  is the average for the problems that are asked to solve, and, if the word for the spin glass model is used,  $[\ ]_J$  is the random configuration average. Therefore, in order to calculate the expectation value of the energy, we sample

$$E = -\frac{J(t)}{\beta} \sum_{\langle ij \rangle} \int_0^\beta d\tilde{t} \tau_{ij} \sigma_i^z(\tilde{t}) \sigma_j^z(\tilde{t}) - \frac{1}{\beta} \sum_{i=1}^N n_{\text{kink}}(i), \quad (25)$$

where  $n_{\text{kink}}(i)$  is the number of kinks on the imaginary time at site  $i$ . The solution of a given optimized problem at site  $i$  can be obtained as

$$S_i^{\text{result}} = \frac{\int_0^\beta d\tilde{t} \sigma_i^z(\tilde{t})}{\left| \int_0^\beta d\tilde{t} \sigma_i^z(\tilde{t}) \right|}. \quad (26)$$

The aim of the quantum annealing is to solve the optimized problems. Therefore, by using Eqs.(2) and (26), investigating an energy  $E_P$  given by

$$E_P = - \sum_{\langle ij \rangle} \tau_{ij} \frac{\int_0^\beta d\tilde{t} \sigma_i^z(\tilde{t})}{\left| \int_0^\beta d\tilde{t} \sigma_i^z(\tilde{t}) \right|} \frac{\int_0^\beta d\tilde{t} \sigma_j^z(\tilde{t})}{\left| \int_0^\beta d\tilde{t} \sigma_j^z(\tilde{t}) \right|} \quad (27)$$

can be suited for this study, since, if a lot of kinks remains in the system after annealing, there is a possibility that  $E$  of Eq. (25) gives an unexpected low value. In addition, there is a possibility that this unexpected low value gives a false impression for success of the quantum annealing. Thus we investigate the expectation value of the energy  $E_P$  instead of the expectation value of the energy  $E$  in this article.

We define the exact ground-state energy of Eq. (2) as  $E_G$ , where the exact ground-state is the exact solution of the problem.  $E_G$  depends on  $\tau_{ij}$ . The residual energy  $E_{\text{res}}$  is given by

$$E_{\text{res}} = [\langle E_P \rangle_T - E_G]_J. \quad (28)$$

We investigate the residual energy  $E_{\text{res}}$  in this article.

The accuracy  $P_{\text{exact}}$  is given by

$$P_{\text{exact}} = [\langle \delta_{E_P, E_G} \rangle_T]_J, \quad (29)$$

where  $\delta$  is the Kronecker delta. We investigate the accuracy  $P_{\text{exact}}$  in this article.

## 6 A new quantum annealing schedule

The mathematical form of the present Monte Carlo algorithm derived in §3 is directly related to the derivation of a smallest effective transverse field, and the quantum annealing schedule that we propose in this article utilizes the field. Firstly, we derive the field based on a discussion of percolation of spin correlation for the continuous-imaginary-time direction of one spin.

By cuts used in Eqs.(19) and (20), spin correlations are cut for the imaginary-time direction. We consider the fewest number of cuts per spin for cutting spin correlations. Since the imaginary-time direction has the periodic boundary conditions, by considering a percolation of spin correlations, the fewest number of cuts per spin,  $n_{\text{fewest cut}}$ , is obtained as two,

$$n_{\text{fewest cut}} = 2. \quad (30)$$

By using Eqs. (22) and (30), the fewest number of cuts for parallel spins on the continuous-imaginary time per spin,  $n_{\text{fewest add}}$ , is obtained as

$$n_{\text{fewest add}} + n_{\text{kink}} = 2. \quad (31)$$

By using Eq.(20), the average number of cuts for parallel spins on the continuous-imaginary time per spin is obtained as

$$\sum_{n_{\text{add}}=0}^{\infty} n_{\text{add}} P(n_{\text{add}}) = \gamma(t)\beta. \quad (32)$$

Therefore, when there is no kink ( $n_{\text{kink}} = 0$ ), by using Eqs. (31) and (32), we obtain a smallest effective transverse field  $\gamma_S$  as

$$\gamma_S = \frac{2}{\beta}. \quad (33)$$

When there are kinks, by using Eq. (31),  $n_{\text{fewest add}}$  is obtained as

$$n_{\text{fewest add}} < 2 \quad (34)$$

since  $n_{\text{kink}} > 0$ . Therefore, when there are kinks, a smallest effective transverse field  $\tilde{\gamma}_S$  is obtained as

$$\tilde{\gamma}_S < \gamma_S. \quad (35)$$

If there is no kink, the transverse field  $\gamma$  for  $\gamma < \gamma_S$  is not effective for generating quantum effect.  $\gamma$  for  $\gamma = \gamma_S$  is effective for generating quantum effect regardless of the number of kinks. A smallest effect transverse field that does not depend on the number of kinks is desired in this study. Therefore, we estimate that  $\gamma_S$  is the smallest effective field that should be used in this study.

We propose a QA schedule for studying transverse-field-based quantum versus classical annealing of the Ising model by utilizing the field  $\gamma_S$  as

$$\gamma(t) = \gamma_S H_E\left(\theta - \frac{t}{T_I}\right) = \frac{2}{\beta} H_E\left(\theta - \frac{t}{T_I}\right), \quad (36)$$

where  $H_E(x)$  is the Heaviside step function, using the half-maximum convention, which gives 1 if  $x > 0$ , gives 0.5 if  $x = 0$ , and gives 0 if  $x < 0$ .  $\theta$  is an adjusting value for  $0 \leq \theta < 1$ . The value  $\theta$  is set to 0.5 for example. Here, in this study,  $t$  is the Monte Carlo time, and  $T_I$  is the ending Monte Carlo time. The present QA schedule is made based on the concept of perturbation theory. For  $J(t)$  in

Eq. (1), using  $J(t) = t/T_I$  for  $0 \leq t \leq T_I$  may be the simplest form as used in Ref. [6]. Therefore, we investigate

$$\mathcal{H}_1(t) = -\frac{t}{T_I} \sum_{\langle ij \rangle} \tau_{ij} \sigma_i^z \sigma_j^z - \frac{2}{\beta} H_E \left( 0.5 - \frac{t}{T_I} \right) \sum_{i=1}^N \sigma_i^x \quad (37)$$

as the present-quantum-annealing schedule in this article. The Hamiltonian  $\mathcal{H}_2(t)$  for a conventional-quantum-annealing schedule is given by [6]

$$\mathcal{H}_2(t) = -\frac{t}{T_I} \sum_{\langle ij \rangle} \tau_{ij} \sigma_i^z \sigma_j^z - \left( 1 - \frac{t}{T_I} \right) \sum_{i=1}^N \sigma_i^x. \quad (38)$$

We also investigate  $\mathcal{H}_2(t)$  as a conventional-quantum-annealing schedule in this article for comparison. As a classical-annealing schedule, we investigate

$$\mathcal{H}_3(t) = -\frac{t}{T_I} \sum_{\langle ij \rangle} \tau_{ij} \sigma_i^z \sigma_j^z \quad (39)$$

in this article. This classical annealing schedule is mathematically the same with a classical annealing for  $J = 1$ ,  $\beta(t) = t/T_I$  and  $\gamma = 0$  in Eq. (6), thus we investigate  $\mathcal{H}_3(t)$ .

In Refs. [3, 10], an another quantum-annealing schedule has also been investigated. The transverse field  $\gamma(t)$  is initially much larger than the couplings,  $\gamma(0) \gg |J_{ij}|$ , and  $J(t)$  is a constant for  $t$ . During QA,  $\gamma(t)$  is slowly reduced to zero. For this annealing schedule, it is reported in Ref. [10] that Monte Carlo simulations for the Ising spin glass model on the square lattice in the physically relevant continuous-imaginary-time limit do not show superiority of QA against CA. We do not investigate this schedule in this article because the results are already shown in Ref. [10].

A method using a pulse of the transverse field is also proposed in Ref. [14], however, the annealing schedule for this method is unclear in Ref. [14]. Thus we do not compare the present annealing schedule with the method using a pulse in this article.

We investigate the effectivities for  $\mathcal{H}_1(t)$ ,  $\mathcal{H}_2(t)$  and  $\mathcal{H}_3(t)$  in this article.

By using Eqs. (22) and (32) on condition of no kink and a fixed number for the number of cuts, the transverse field is quantized as

$$\gamma_Q(n) = \frac{n}{\beta}, \quad n = 2, 3, 4, \dots, \quad (40)$$

in the Ising model for generating quantum effect. Even if a transverse field  $\gamma_Q(n)$  is imposed, the quantum effect increases with increasing the number of kinks. However, to know that the transverse field is quantized as in Eq. (40) can be convenient for adjustment of the quantum effect.  $\gamma_Q(2)$  is the smallest effective field used in this study ( $\gamma_Q(2) = \gamma_S$ ). If a transverse field  $\gamma_Q$  for  $n = 3$  is imposed, the generation of quantum effect for  $n = 3$  is guaranteed at least.

When a transverse field  $\gamma_{\text{ex}}$  is imposed for example, the quantum number  $n_{\text{ex}}$  is obtained as  $n_{\text{ex}} = \beta\gamma_{\text{ex}}$ . If  $n_{\text{ex}} < 2$ ,  $\gamma_{\text{ex}}$  is estimated as no effective for generating quantum effect. If  $n_{\text{ex}} \geq 2$ , the generation of quantum effect for  $n_{\text{ex}}$  is guaranteed at least. Since very large  $n$  disorders spin orders too much, searching proper  $n$  for time  $t$  is, of course, required for good performance of optimization. This quantization is a quantization for the number of cutting spin correlation on the continuous-imaginary-time direction of one spin. Because the quantum effect by the transverse field depends on the correlation lengths on the continuous-imaginary-time direction, we focus on this quantization, and we utilize the fewest quantum number in this article.

## 7 Simulation results

We firstly tested our program source code for the two-spin-model case in order to fix software bugs, because static properties in the two-spin model are exactly calculated. We secondly tested our program source code for the one-dimensional ferromagnetic Ising spin chain with periodic boundary conditions under the transverse field ( $\tau_{ij} = 1$  and  $\gamma(t) = \gamma$ ) in order to fix software bugs. The critical properties at  $T_E = 0$  are identical to those of the classical two-dimensional Ising model and are well known exactly (the critical exponents are  $\gamma_C = 1$ ,  $\nu = 1$ ,  $\beta = 1/8$  and  $z = 1$ ) [21]. We confirmed the values of the critical exponents  $\nu$  and  $\beta$  by using the present algorithm and the finite-size-scaling method. We do not show the results of the two-spin-model case and the one-dimensional-ferromagnetic-Ising-spin-chain case, because the simulations were performed for fixing software bugs. Software bugs are fixed as above.

Next, we performed simulations for the  $\pm J$  Ising spin glass model on the square lattice. For each system size, 100 realizations of  $\tau_{ij}$  were investigated. For each realization, 10 simulations were performed. Thus, 1000 simulations were performed for each system size. 100 Monte Carlo steps were used for preparing the initial states at each simulation. The inverse temperature  $\beta$  was set to  $\beta = 10$ . The CA schedule, the conventional-quantum-annealing (CQA) schedule, and the present-quantum-annealing (PQA) schedule were performed. All the instances used for CA, CQA and PQA are the same.

Fig. 3 shows the relation between the ending Monte Carlo time  $T_I$  and the residual energy  $E_{\text{res}}$  given in Eq. (28). The number of spins,  $N$ , is 100. The solid square represents the result for the CA schedule, the solid circle represents the result for the CQA schedule, and the open circle represents the result for the PQA schedule. At  $T_I = 200$ , the result of CA is better than the results of CQA and PQA. At  $T_I = 1600$ , the results of CQA and PQA are better than the result of CA. Therefore, by fast annealing, CA is seen to outperform QA, but, by slow annealing, QA is seen to outperform CA. At  $T_I = 200$  and  $T_I = 400$ , the results of PQA are better than the results of CQA. When examining errorbars, we could not distinguish the results of PQA from the results of CQA at  $T_I = 800$  and  $T_I = 1600$ . Thus, PQA has the same effectivity with CQA at  $T_I = 800$  and  $T_I = 1600$ .

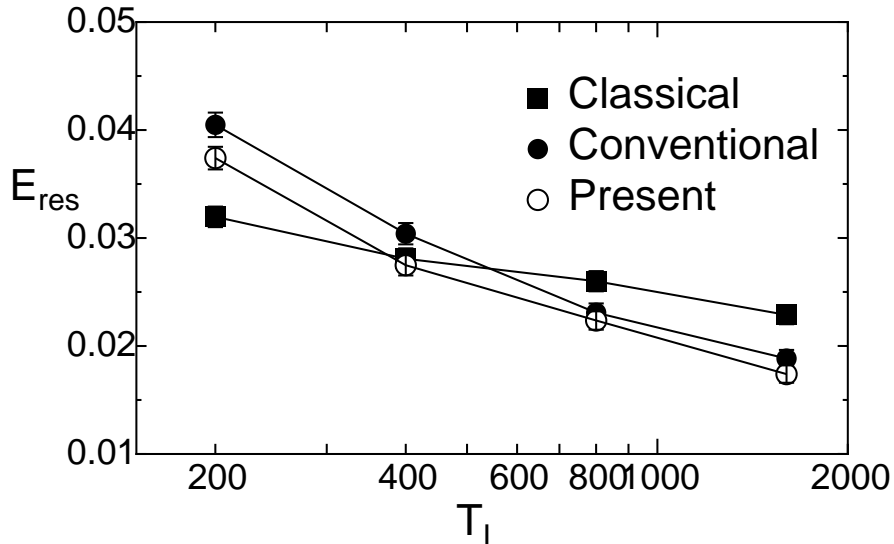


Figure 3: The relation between the ending Monte Carlo time  $T_I$  and the residual energy  $E_{\text{res}}$ . The results of the  $\pm J$  Ising spin glass model on the square lattice are shown. The number of spins,  $N$ , is 100, and the inverse temperature  $\beta$  is 10. The solid square represents the result for the classical-annealing schedule, the solid circle represents the result for the conventional-quantum-annealing schedule, and the open circle represents the result for the present-quantum-annealing schedule.

Fig. 4 shows the relation between the ending Monte Carlo time  $T_I$  and the accuracy  $P_{\text{exact}}$  given in Eq. (29). The number of spins,  $N$ , is 100. The solid square represents the result for the CA schedule, the solid circle represents the result for the CQA schedule, and the open circle represents the result for the PQA schedule. At  $T_I = 200$ , the result of CA is better than the results of CQA and PQA. At  $T_I = 1600$ , the results of CQA and PQA are better than the result of CA. Therefore, by fast annealing, CA is seen to outperform QA, but, by slow annealing, QA is seen to outperform CA. At  $T_I = 400$  and  $T_I = 1600$ , the results of PQA are better than the results of CQA. When examining errorbars, we could not distinguish the results of PQA from the results of CQA at  $T_I = 200$  and  $T_I = 800$ . Thus, PQA has the same effectivity with CQA at  $T_I = 200$  and  $T_I = 800$ .

From Figs. 3 and 4, by fast annealing, CA is seen to outperform QA, but, by slow annealing, QA is seen to outperform CA. From Figs. 3 and 4, PQA is seen to outperform CQA, although some results are not distinguished.

Fig. 5 shows the relation between the number of spins,  $N$ , and the residual energy  $E_{\text{res}}$  given in Eq. (28). The ending Monte Carlo time  $T_I$  is 1600. The solid square represents the result for the CA schedule, the solid circle represents

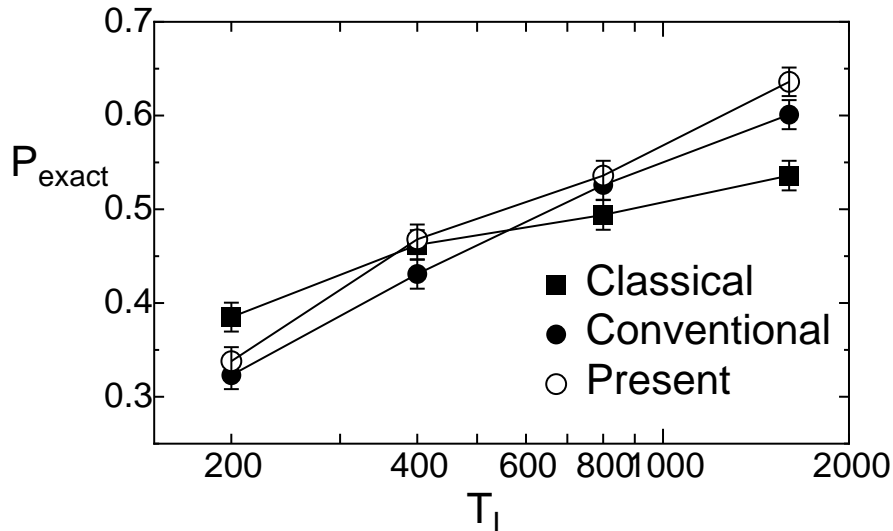


Figure 4: The relation between the ending Monte Carlo time  $T_I$  and the accuracy  $P_{\text{exact}}$ . The results of the  $\pm J$  Ising spin glass model on the square lattice are shown. The number of spins,  $N$ , is 100, and the inverse temperature  $\beta$  is 10. The solid square represents the result for the classical-annealing schedule, the solid circle represents the result for the conventional-quantum-annealing schedule, and the open circle represents the result for the present-quantum-annealing schedule.

the result for the CQA schedule, and the open circle represents the result for the PQA schedule. At  $N = 16$ , when examining errorbars, we could not distinguish the result of QA from the result of CA. Thus, QA has the same effectivity with CA at  $N = 16$ . At  $N = 100$ , the result of QA is better than the result of CA. QA is seen to outperform CA at large system size. At  $N = 16$ ,  $N = 64$  and  $N = 100$ , when examining errorbars, we could not distinguish the results of PQA from the results of CQA. Thus, PQA has the same effectivity with CQA at  $N = 16$ ,  $N = 64$  and  $N = 100$ . At  $N = 36$ , the result of PQA is better than the result of CQA. We can see that the results of CQA and PQA are better than the result of CA for  $N$  dependence. This shows the superiority of QA against CA. We could not see the superiority of PQA against CQA for  $N$  dependence.

Fig. 6 shows the relation between the number of spins,  $N$ , and the accuracy  $P_{\text{exact}}$  given in Eq. (29). The ending Monte Carlo time  $T_I$  is 1600. The solid square represents the result for the CA schedule, the solid circle represents the result for the CQA schedule, and the open circle represents the result for the PQA schedule. At  $N = 16$ , when examining errorbars, we could not distinguish the result of QA from the result of CA. Thus, QA has the same effectivity with CA at  $N = 16$ . At  $N = 100$ , the result of QA is better than the result of CA.

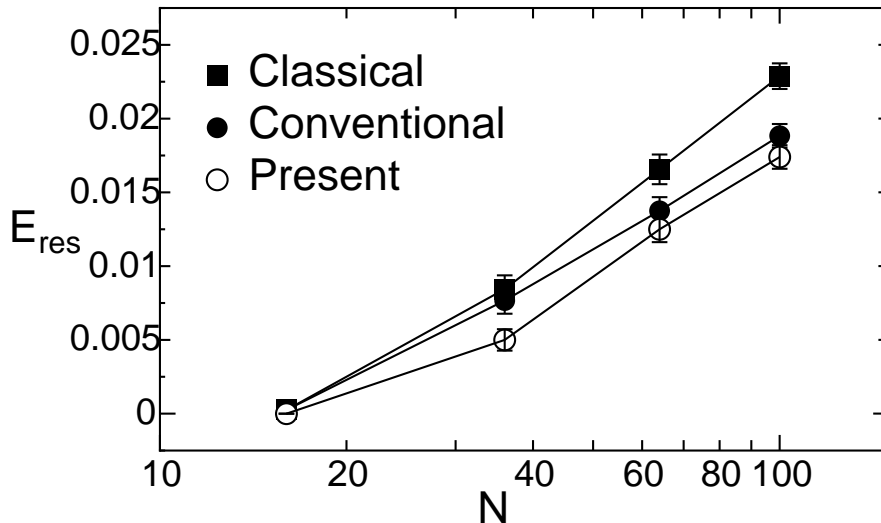


Figure 5: The relation between the number of spins,  $N$ , and the residual energy  $E_{\text{res}}$ . The results of the  $\pm J$  Ising spin glass model on the square lattice are shown. The ending Monte Carlo time  $T_I$  is 1600, and the inverse temperature  $\beta$  is 10. The solid square represents the result for the classical-annealing schedule, the solid circle represents the result for the conventional-quantum-annealing schedule, and the open circle represents the result for the present-quantum-annealing schedule.

QA is seen to outperform CA at large system size. At  $N = 16$  and  $N = 64$ , when examining errorbars, we could not distinguish the results of PQA from the results of CQA. Thus, PQA has the same effectivity with CQA at  $N = 16$  and  $N = 64$ . At  $N = 36$  and  $N = 100$ , the results of PQA are better than the results of CQA. We can see that the results of CQA and PQA are better than the result of CA for  $N$  dependence. This shows the superiority of QA against CA. We could not see the superiority of PQA against CQA for  $N$  dependence.

From Figs. 5 and 6, QA is seen to outperform CA for performance of optimization for the dependence of the number of spins. From Figs. 5 and 6, PQA is seen to outperform CQA, although some results are not distinguished.

## 8 Concluding remarks

We performed Monte Carlo simulations for the spin glass model on the square lattice. As the simulation results, QA was seen to outperform CA when the annealing time was spent enough. As the simulation results, QA was seen to outperform CA for performance of optimization for the dependence of the number of spins when the annealing time was spent enough. Therefore, our

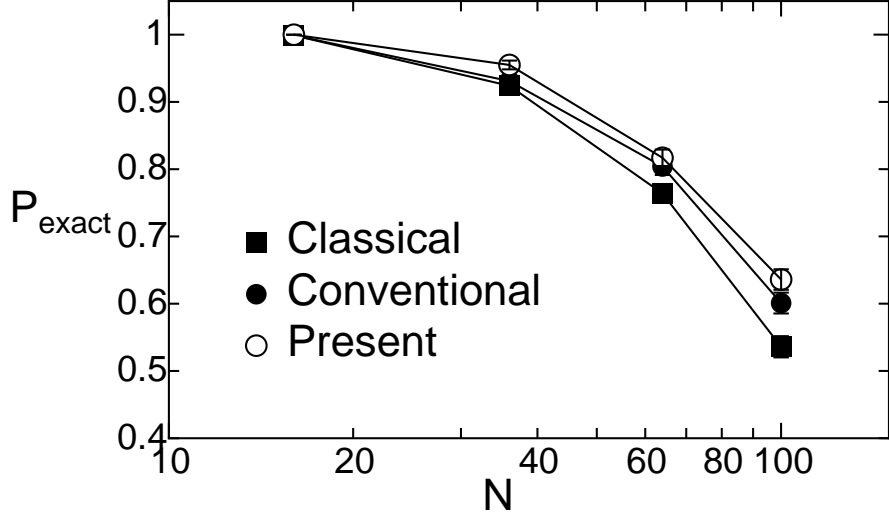


Figure 6: The relation between the number of spins,  $N$ , and the accuracy  $P_{\text{exact}}$ . The results of the  $\pm J$  Ising spin glass model on the square lattice are shown. The ending Monte Carlo time  $T_I$  is 1600, and the inverse temperature  $\beta$  is 10. The solid square represents the result for the classical-annealing schedule, the solid circle represents the result for the conventional-quantum-annealing schedule, and the open circle represents the result for the present-quantum-annealing schedule.

conclusion is that there is a superiority of QA against CA for the spin glass model by using Monte Carlo simulations.

QA was seen to outperform CA for performance of optimization for the system-size dependences. However, we were not able to numerically estimate the system-size dependences for the results, because the dependences were not clear enough. Although the estimations for the system-size dependences would be hard tasks, the estimations are tasks for the future.

Conventionally, changing the temperature  $T_E$  with a fixed  $J(t)(= J)$  and no  $\gamma(t)$  term of Eq. (1) is called CA, however, in this article, we called that changing  $J(t)$  with a fixed  $T_E$  and no  $\gamma(t)$  term of Eq. (1) is CA. There are two reasons. One is that changing  $T_E$  with a fixed  $J$  and no  $\gamma(t)$  term is mathematically the same with changing  $J(t)$  with a fixed  $T_E$  and no  $\gamma(t)$  term. One is that changing  $J(t)$  with a fixed  $T_E$  and no  $\gamma(t)$  term is more practical in relation to the D-Wave chip[9]. These may be trivial, but we consider that these are also significant for understanding quantum annealing computing.

The size of the transverse field used in the conventional QA schedule is larger than the size of that used in the present QA schedule, however, as the simulation results, the present QA schedule was more effective than the conventional QA

schedule. The reason may be that very large transverse field disorders spin orders too much, thus the relaxation time for the disorders can be required, although the tunneling effect by the transverse field helps to make the systems escape from local minima of the free energy. Therefore, this means that a thorough investigation for setting of QA schedule is needed. This can be an important task for the future.

Very recently, it is reported in Ref. [22] that, by fast annealing, QA is seen to outperform CA for their benchmark spin-glass problems. On the other hand, our results showed that, by slow annealing, QA is seen to outperform CA for our benchmark spin-glass problems. Since the used annealing schedules and the used models are different, we can not say anything for the differences between the results, but they have also proposed a way of comparing QA with CA. Their schedule uses observables, on the other hand, our schedule uses a smallest effective field. Their schedule can be a better schedule, however their schedule depends on models. On the other hand, our schedule does not depend on models. For this difference between the QA schedules, we believe that the present study is also significant. The detailed comparison is a task for the future.

Other quantum annealing schedules using the smallest effective field derived in this article may also be worth considering. The present QA schedule is made based on the concept of perturbation theory. Other quantum annealing schedules using the smallest effective field based on the same concept can also be considered, and some schedules among them may be better for performance of optimization.

A set of the computer program source codes used in this article will be on sale in [23] due to several reasons.

## Acknowledgments

The spin glass server [24] was used to obtain the ground-state energies for realizations. We thank the persons concerned with the spin glass server.

## References

- [1] P. Ray, B. K. Chakrabarti and A. Chakrabarti, *Phys. Rev. B* **39** (1989) 11828.
- [2] A. B. Finnila, M. A. Gomez, C. Sebenik, C. Stenson, J. D. Doll, *Chem. Phys. Lett.* **219** (1994) 343.
- [3] T. Kadowaki and H. Nishimori, *Phys. Rev. E* **58** (1998) 5355.
- [4] G. Santoro and E. Tosatti, *J. Phys. A: Math. Gen.* **39** (2006) R393.
- [5] A. Das and B. K. Chakrabarti, *Rev. Mod. Phys.* **80** (2008) 1061.
- [6] E. Farhi, J. Goldstone, S. Gutmann and M. Sipser, arXiv:quant-ph/0001106.

- [7] E. Farhi, J. Goldstone, S. Gutmann, J. Lapan, A. Lundgren and D. Preda, *Science* **292** (2001) 472.
- [8] S. Geman and D. Geman, *IEEE Trans. Pattern Anal. Mach. Intell.* **6** (1984) 721.
- [9] M. W. Johnson, M. H. S. Amin, S. Gildert, T. Lanting, F. Hamze, N. Dickson, R. Harris, A. J. Berkley, J. Johansson, P. Bunyk, E. M. Chapple, C. Enderud, J. P. Hilton, K. Karimi, E. Ladizinsky, N. Ladizinsky, T. Oh, I. Perminov, C. Rich, M. C. Thom, E. Tolkacheva, C. J. S. Truncik, S. Uchaikin, J. Wang, B. Wilso and G. Rose, *Nature* **473** (2011) 194.
- [10] B. Heim, T. F. Rønnow, S. V. Isakov and M. Troyer, *Science* **348** (2015) 215.
- [11] B. Derrida, *Phys. Rep.* **184** (1989) 207.
- [12] A. T. Ogielski, *Phys. Rev. B* **32** (1985) 7384.
- [13] H. Rieger and N. Kawashima, *Euro. Phys. J. B* **9** (1999) 233.
- [14] S. Morita, S. Suzuki and T. Nakamura, *Phys. Rev. E* **79** (2009) 065701.
- [15] S. F. Edwards and P. W. Anderson, *J. Phys. F* **5** (1975) 965.
- [16] M. Mézard, G. Parisi and M. A. Virasoro, *Spin Glass Theory and Beyond* (World Scientific, Singapore, 1987).
- [17] H. Nishimori, *Statistical Physics of Spin Glasses and Information Processing: An Introduction* (Oxford University Press, Oxford, UK, 2001).
- [18] N. Kawashima and H. Rieger, Recent progress in spin glasses, in *Frustrated Spin Systems*, ed. H. T. Diep (World Scientific, Singapore, 2004).
- [19] M. Suzuki, *Prog. Theor. Phys.* **56**, 1454 (1976).
- [20] N. Kawashima and J. E. Gubernatis, *Phys. Rev. E* **51** (1995) 1547.
- [21] B. M. McCoy and T. T. Wu, *The two-dimensional Ising model*, Harvard University Press, Cambridge, Massachusetts, (1973).
- [22] D. Herr, E. Brown, B. Heim, M. Könz, G. Mazzola and M. Troyer, arXiv:1705.00420.
- [23] <http://www.to-qc.com/services/>.
- [24] <http://www.informatik.uni-koeln.de/spinglass/>.